Advanced avrami formula and its application to describing the isothermal crystallisation of polymers

Vas L. M., Slezák E., Molnár K., Ronkay F. Gy.

Thermochimica Acta 746 (2025) 179950

Contents lists available at ScienceDirect

Thermochimica Acta

journal homepage: www.elsevier.com/locate/tca

Advanced avrami formula and its application to describing the isothermal crystallisation of polymers

László Mihály Vas [a], Emese Slezák [b,c], Kolos Molnár [a,d,e,*], Ferenc Ronkay [c]

[a] Department of Polymer Engineering, Faculty of Mechanical Engineering, Budapest University of Technology and Economics, Műegyetem rkp. 3., H-1111, Budapest, Hungary
[b] Department of Organic Chemistry and Technology, Faculty of Chemical Technology and Biotechnology, Budapest University of Technology and Economics, Műegyetem rkp. 3., H-1111, Budapest, Hungary
[c] Imsys Engineering Services Ltd., Mozaik street 14/A., H-1033, Budapest, Hungary
[d] HUN-REN–BME Research Group for Composite Science and Technology, Műegyetem rkp. 3, H-1111, Budapest, Hungary
[e] MTA-BME Lendület Sustainable Polymers Research Group, Műegyetem rkp. 3, H-1111, Budapest, Hungary

ARTICLE INFO

Keywords:
Avrami equation
Crystallisation of polymers
Instantaneous and random nuclei
Instantaneous-nuclei-based crystalline fraction

ABSTRACT

The classic Avrami formula has widely been used to describe and characterize the crystallisation process of polymers. We showed that the Avrami formula is not correct for the random nucleation. To eliminate this and some problems of fitting the Avrami formula with integer exponent revealed in the literature, we modified the Avrami equation and derived a new extended formula that can describe instantaneous and random (time-dependent) nucleation simultaneously. This formula may give information on the crystalline structure of both types of nuclei; moreover, it makes it possible to determine the crystalline fraction developed from the instantaneous nuclei. The latter enables us to estimate, for example, the effect of nucleating agents numerically on the crystallisation process and the ultimate crystallinity. The applicability of the new formula was validated by performing isothermal crystallisation tests on poly(ethylene-terephthalate) (PET), polypropylene (PP), low- and high-density polyethylene (LDPE and HDPE) samples at various temperatures, which resulted in a better fit characterized by the much smaller relative maximum absolute error (0.4–2.9 %) related to that for the Avrami equation (1.9–15.9 %).

1. Introduction

Semi-crystalline polymers – unlike amorphous materials – contain crystalline (ordered) phase domains when solidified. Semi-crystalline polymers generally exhibit a spherulitic microstructure [1]. The crystalline fraction of semi-crystalline polymers, in general, provides higher stiffness and tensile strength [2–5]. Due to these favourable properties, semi-crystalline polymers have a wide range of applications where good heat resistance and mechanical properties are required; they are applied, e.g., in the automotive industry or as synthetic fibres [6,7]. There are several representatives among the most frequently used, so-called commodity plastics: polyethylene (PE), polypropylene (PP) and poly(ethylene-terephthalate) (PET).

The crystallisation of polymers can be separated into two steps: the first step is the formation of crystal nuclei, and the second one is crystal growth [8]. The degree of crystallisation increases in a strictly monotonic way over time [9,10], and the rate of cooling and the temperatures have the highest impact [11,12] on the process.

Isothermal crystallisation leads to the formation of spherulites, which consist of non-crystalline regions and crystalline lamellae [13]. The growth of spherulites is unrestricted before the encounter of their fronts during primary crystallisation. The secondary phase crystallisation leads to lamellar growth and the thickening of crystals and growth is mainly limited to the inter-spherulitic regions [14]. The process is linear with time in the primary phase, while it varies with the square root of time during secondary crystallisation [15].

Compared to isothermal crystallisation, the fronts of growing spherulites meet during crystallisation and inhibit one another's growth. The chain parts in the already-crystallised lamellae inhibit the movement of segments in the molten state, thus resulting in a kinetic obstacle

* Corresponding author at: Department of Polymer Engineering, Faculty of Mechanical Engineering, Budapest University of Technology and Economics, Műegyetem rkp. 3., H-1111, Budapest, Hungary.
E-mail address: molnar@pt.bme.hu (K. Molnár).

https://doi.org/10.1016/j.tca.2025.179950
Received 2 October 2024; Received in revised form 31 January 2025; Accepted 3 February 2025
Available online 4 February 2025

Table 1
Relation between the Avrami exponent and the nucleation [24,25].

Growth + nucleation	n_A
Spherulitic (3D) growing + random nucleation	3+1=4
Spherulitic (3D) growing + instantaneous nucleation	3+0=3
Disc-like (2D) growing + random nucleation	2+1=3
Disc-like (2D) growing + instantaneous nucleation	2+0=2
Rod-like (1D) growing + random nucleation	1+1=2
Rod-like (1D) growing + instantaneous nucleation	1+0=1

for crystallisation.

The speed of crystallisation is determined by kinetic and thermodynamic properties: at high temperatures, the molecules are mobile, but the thermodynamic driving force is small. By decreasing the temperature, undercooling and the driving force increase, resulting in faster spherulite growth, but at a certain point, the speed reaches a maximum. Further, decreasing the temperature decreases the mobility of polymer chains, growth becomes kinetically inhibited, and the speed decreases [16,17].

The Avrami equation, also known as the Kolmogorov-Johnson-Mehl-Avrami equation is a simple empirical model which describes the crystallisation process of various materials (metals, polymers, etc.) under isothermal conditions. The model has several limitations – for example, it assumes a homogeneous nucleation with spherical nuclei. Another problem is that two different formulae are needed for the instantaneous and the random nucleation. In general, both instantaneous and random nucleation takes place simultaneously. That is why, throughout the decades, several researchers attempted to modify the classical Avrami equation.

Berlic and Barna [18] extended the well-known model to a multi-dimensional space to describe sporadic polymer crystallisation. They concluded that regardless of the space dimensionality, the Avrami equation has a universal behaviour. Sugio et al. [19] altered the theory by defining a 3-dimensional local number and the probability of its distribution. It was proved that the modified Avrami model can describe the clustering spatial distribution, irrespective of the size distribution of newly formed grains. The classical model cannot meet the protocols of non-random nucleation kinetics. The reason of non-randomness can be the vapor deposition over a surface or the presence of thermal or concentration gradients [20,21]. These gradients might locally influence the rate of nucleation.

Pineda et al. [22] generalized the formula, and the model was suitable for explaining the non-randomness, even when immense regions were affected around the growing grains. Chiari et al. [23] analysed the isothermal crystallisation of propylene-ethylene random copolymers. According to the authors, the classical Avrami model was not suitable for describing the behaviour of the polymorphic system. Instead, a two-stage model was developed which could describe the relation of α and γ lamellae during crystallisation.

The greatest importance of the Avrami formula is – besides the description of the crystallisation process – that by the integer Avrami exponents it gives information about the geometry of the random or instantaneous nuclei and the crystallites. Considering the derivation, this is based on the initial asymptote. According to some of the actual experiences [24–30], the measured crystallisation curve becomes flatter than that given by the Avrami formula, and the fitted exponent is often not an integer, indicating both instantaneous and random nucleation takes place.

As we mentioned above, the Avrami formula has several limitations. It has successfully been applied in many cases to describe or just characterize the crystallisation process, mainly when the exponent might be non-integer, while any of its modifications or other related formulae have not gained wider usage. In the derivation of the Avrami equation, the crystallisation-caused decrease of the melt volume was applied as a global mean effect to describe the spatial hindering and blocking of the growing of the nuclei and the crystals. We, therefore, thoroughly studied its derivation and found that it could be improved to agree better with the measurements. Correspondingly, the objectives of our paper are to:

- Modify the Avrami formula by improving its derivation retaining the role and meaning of the Avrami exponents.
- Extend the modified formula for both the instantaneous and random nucleation resulting in mono- or polymorphic crystallinity.
- Derive a simple formula that describes crystallisation of polymers more precisely.
- This paper is limited to the study of the crystallisation behaviour of polymeric materials. For the validation of the model, we chose LDPE, HDPE, PP and PET materials, which are the most abundant semi-crystalline plastics.

2. Theoretical considerations

2.1. Avrami equation

When reaching the crystallisation temperature during the cooling of a polymer melt (capable of crystallisation) ***instantaneous nuclei*** formation happens and solidification begins. These nucleation sites (in general on the surface of the container or filling particles and fibres) develop into growing crystalline parts. In the meantime, at random places of molecular densification in the melt, so-called ***random nuclei*** form that may also develop into crystalline parts [24–28].

The solidifying process of the crystalline mass fraction as a function of time, $x_A(t)$, has usually been described by the mass-normalized ***Avrami equation*** [24–28] (see Supplementary materials A1) as follows (t≥0), (1):

$$x_A(t) = \frac{m_S(t)}{m_0} = 1 - e^{-x_{0A}(t)} = 1 - e^{-Z_A t^{n_A}} \underset{t\to 0}{\sim} x_{0A}(t) = Z_A t^{n_A} = \left(\frac{t}{t_A}\right)^{n_A} \quad (1)$$

where m_0 is the mass of the polymer melt, $m_S(t)$ is the mass of the solidifying crystalline parts, $x_{0A}(t)$ is the initial asymptote that is a simple power function, and finally Z_A, t_A, and n_A are the speed constant, the scale factor, and the Avrami exponent (index A), respectively. The Avrami exponent, n_A, is an integer and relates to the geometry, dimension (d), and type of the nucleus development (Table 1) which makes the Avrami equation particularly important [24,25], (2):

$$n_A = \begin{cases} n_{A1} = d + 1, & \textit{random nucleus formation} \\ n_{A0} = d + 0, & \textit{instantaneous nucleus formation} \end{cases} \quad (2)$$

The Avrami equation is a phenomenological model, and it was derived by using the view of the probability theory. The simplicity of the model made it popular and may be overused [29] for describing the kinetics of isothermal crystallisation. However, the limitations of the model were well-known, because of the initial assumptions, such as that the nucleus size is infinitely small, and the nuclei are randomly distributed within the melt volume.

Fig. 1 shows the graph of the Avrami Eq. (1) at different exponents (n_A) (Fig. 1.a) and the fitting of the exponent functions ($x_{0A}(t)$) as initial asymptotes at the initial part of the crystallisation process (Fig. 1.b).

Let ρ_L and ρ_S be the density of the polymer melt (liquid) and the solid crystal, respectively. Suppose that the growth rate, $\dot{L}_0$, is constant, hence it can be called the *growth constant*. When the ***random nucleus*** is either 3D spheroidal, or 2D disc-shaped (l_1=l_2=r, l_3=h), or 1D rod-like (l_1=l, $l_2 \cdot l_3$=A_0) then its volume $v_1(t)$, the crystalline mass fraction $x_{0A1}(t)$, and the corresponding speed constant Z_{A1} in the initial part of the crystallisation are as follows [24,25] (for calculating $x_{0Ai}(t)$, i=0 or 1, see Supplementary materials A1), (3):

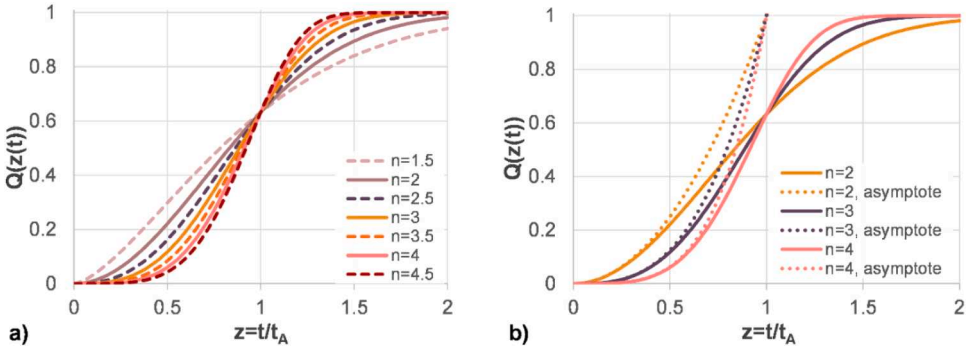

Fig. 1. *Graphical form of the Avrami equation* $Q(z(t))=x_A(t)$ *for integer and real exponents (a) and the initial asymptotes* $x_{0A}(t)$ *for integer exponents (b) (*$n=n_A$ *if n is integer) as a function of the normalized time* $z=t/t_0$.

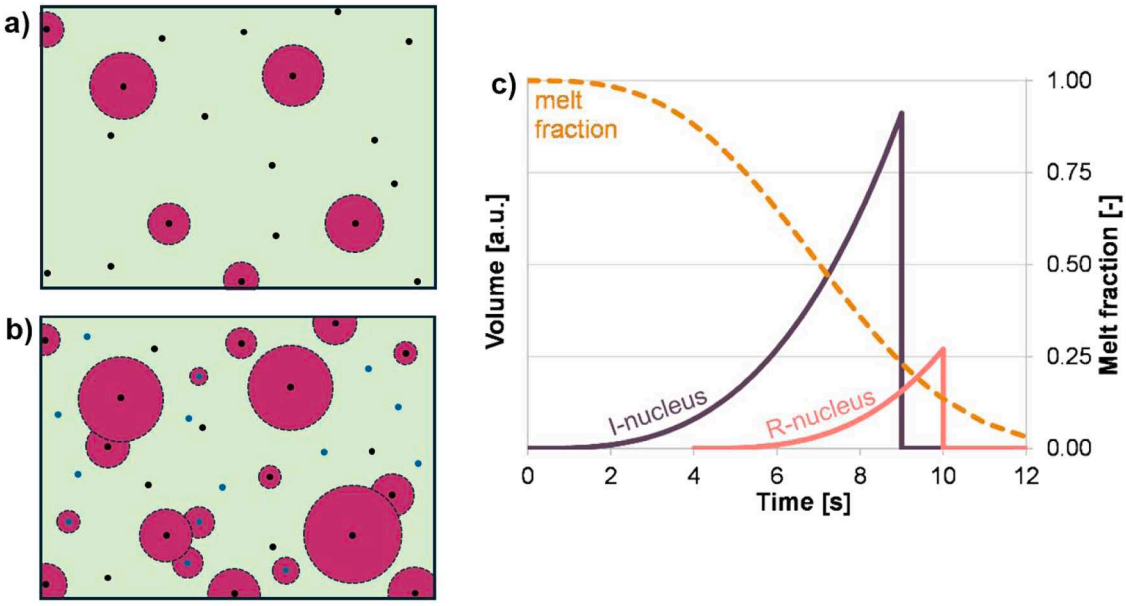

Fig. 2. Conceptual diagram on the development and limitation of single spherical instantaneous and random nuclei illustrating the global spatial limitation effect. a) Formation of instantaneous nuclei (black) due to surface roughness and nucleating agents, b) Crystal growth, random nuclei formation (blue) and spatial hindrance, c) the development and limitation of single spherical instantaneous (I-nucleus: $\tau_0=0$, $\tau_1=9$) and random (R-nucleus: $\tau_0=4$, $\tau_1=10$).

$$v_1=\begin{cases}3D: \ \frac{4\pi}{3}r^3=\frac{4\pi}{3}(\dot{L}_0t)^3\\ 2D: \ \pi hr^2=\pi h(\dot{L}_0t)^2\\ 1D: \ A_0l=A_0(\dot{L}_0t)\end{cases}\Rightarrow x_{0A1}(t)=\begin{cases}3D: \ \frac{\rho_S}{\rho_L}\frac{\dot{P}_0(\dot{L}_0)^3\pi}{3}t^4\\ 2D: \ \frac{\rho_S}{\rho_L}\frac{\dot{P}_0(\dot{L}_0)^2\pi h}{3}t^3\\ 1D: \ \frac{\rho_S}{\rho_L}\frac{\dot{P}_0\dot{L}_0A_0}{2}t^2\end{cases}\Rightarrow Z_{A1}$$

$$=\begin{cases}3D: \ \frac{\rho_S}{\rho_L}\frac{\dot{P}_0(\dot{L}_0)^3\pi}{3}\\ 2D: \ \frac{\rho_S}{\rho_L}\frac{\dot{P}_0(\dot{L}_0)^2\pi h}{3}\\ 1D: \ \frac{\rho_S}{\rho_L}\frac{\dot{P}_0\dot{L}_0A_0}{2}\end{cases} \tag{3}$$

where $\dot{P}_0$ is the random specific *nucleation rate* (the number of nuclei formed in a unit volume and a unit time) and $p(t)=\dot{P}_0t$ is the number of nuclei formed in a unit volume during time, *t*. In the case of instantaneous nuclei $p=P_0$ ($t>0$) where P_0 is the number per unit volume of the nuclei formed instantaneously. Parameters P_0 and $\dot{P}_0$ are constants.

Hence, the form of the formulae for $x_{0A}(t)$ and Z_A in Eq. (3) modifies in the case of the ***instantaneous nuclei*** [24,25], (4):

$$v_0=\begin{cases}3D: \ \frac{4\pi}{3}r^3=\frac{4\pi}{3}(\dot{L}_0t)^3\\ 2D: \ \pi hr^2=\pi h(\dot{L}_0t)^2\\ 1D: \ A_0l=A_0(\dot{L}_0t)\end{cases}\Rightarrow x_{0A0}(t)=\begin{cases}3D: \ \frac{\rho_S}{\rho_L}\frac{P_0(\dot{L}_0)^3\pi}{3}t^3\\ 2D: \ \frac{\rho_S}{\rho_L}\frac{P_0(\dot{L}_0)^2\pi h}{3}t^2\\ 1D: \ \frac{\rho_S}{\rho_L}\frac{P_0\dot{L}_0A_0}{2}t^1\end{cases}\Rightarrow Z_{A0}$$

$$=\begin{cases}3D: \ \frac{\rho_S}{\rho_L}\frac{P_0(\dot{L}_0)^3\pi}{3}\\ 2D: \ \frac{\rho_S}{\rho_L}\frac{P_0(\dot{L}_0)^2\pi h}{3}\\ 1D: \ \frac{\rho_S}{\rho_L}\frac{P_0\dot{L}_0A_0}{2}\end{cases} \tag{4}$$

In some cases, the Avrami equation can be excellently used for describing and understanding the measured crystallisation process [24,25,30], however, according to some other experiences and studies the Avrami equation has not provided proper information on the shape of

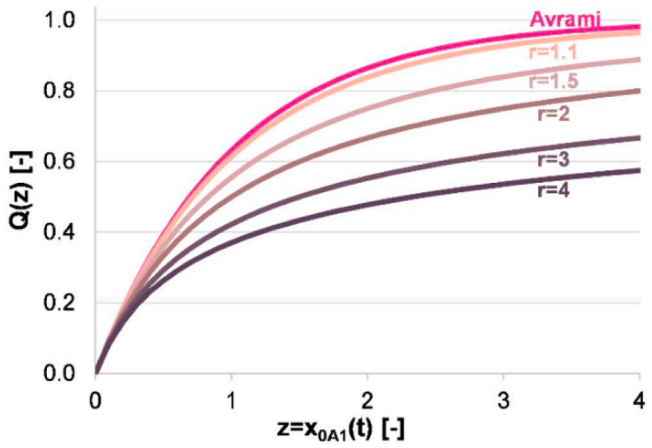

Fig. 3. Comparison of the original Avrami formula and its modified version with different correction exponents (r) versus the exponent function z=x_{0A1}(t).

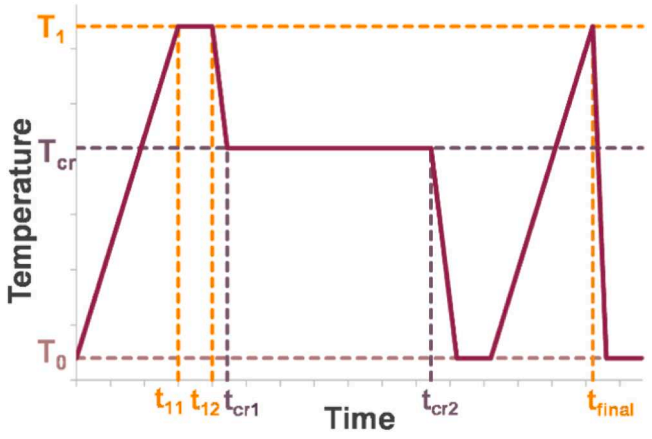

Fig. 4. Thermal controlling program used at the isothermal and non-isothermal DSC measurements of the polymer materials tested.

Table 2
Parameters of the DSC thermal program for the polymer materials tested.

Material	T_0 [°C]	$\beta_1=\beta_4$ [K/min]	T_1 [°C]	$t_1=t_3$ [min]	$\beta_2=\beta_3$ [K/min]	$T_2=T_{cr}$ [°C]	t_2 [min]
PET (vPET and rPET)	20	20	320	5	−50	210 220	30
PP			240			120 130 133 135	
LDPE			220			106.0 106.5 107.0 107.5	
HDPE			220			127.0 127.5 128.0	

the nuclei and/or the Avrami exponent has turned up not as an integer, but a different, real value [24–28]. In several cases, it proved valid only for the initial progressive increasing part of the crystallisation curve, indicating that the fitted exponent significantly differs from the integer Avrami values [24–26], as it was demonstrated by diagrams in Wunderlich's book [26].

In Strobl's opinion [27,28], although the Avrami equation is popular, and it has often been applied to reasonable representation of the measured data, it has relatively rarely given the expected results. Among others, the deviations may be caused for example by the growth of various nuclei of different shapes [24,25].

In general, the estimated Avrami parameters n_A and Z_A are obtained from fitting the linearized Avrami formula to the measurement, $x_{meas}(t)$ where in general the exponent, n_A, is not an integer. The linear relationships (LogLogLin) obtained by double logarithm used for calculations are as follows [24,25,27], and we refer to this model as *Non-integer Avrami formula* in the following sections:

$$Y := lg[-ln(1-x_{meas}(t))] = lgZ_A + n_A lgt =: B + n_A X;\ B = lgZ_A,\ X = lgt \tag{5}$$

$$Z_A = 10^B,\ t_A = 10^{-\frac{B}{n}} \tag{6}$$

2.2. Modified avrami equation for random nuclei

Nucleation is a stochastic process where the starting (τ_0) and end-points (τ_1) of nucleus growth are finite and non-negative stochastic time-variables. In the case of the instantaneous nuclei formation τ_0=0, while τ_0>0 for the random nuclei formation (Fig. 2). The termination of the growth is caused by local steric hindrance realized by another adjacent nucleus, growing crystalline structure or amorphous polymer chains or chain segments. The local spatial hindrance becomes greater and greater with the decreasing volume of the melt (Fig. 2: $v(t)=Ct^3$, $C=1/s^3$, the volume unit is arbitrary). The duration of growth (τ_1-τ_0), hence the volume of the nuclei or crystallites, are stochastic variables, as well. Consequently, crystallinity is given by the fraction of the sum of the nuclei and crystallites at any time.

The spatial constraints for crystalline growth used in the derivation of the Avrami Eq. (1) can be considered adequate for the instantaneous nuclei formation (see Supplementary materials A1); however, in the case of the random nuclei development, time constrains take place as well. Therefore, the Avrami equation should be modified for random nuclei (see Supplementary materials A2) to get a more precise output.

During our research, we applied three concepts regarding the possible modification of the equation for random nuclei. These concepts differ from each other in that at which structural level the modification regarding the temporal effect was inserted in the original derivation (see Supplementary materials A1). Concerning concepts I, II, and III, the related structural levels essentially correspond to the global, intermediate, and local views of the crystallisation process, respectively. In the derivation of the Avrami formula, global spatial constrains were applied.

Concept I (index *I, global approach*), (7), lead to an explicit, well-functioning result, $x_{Ir}(t)$, (as a default: r-1=α≈1/3):

$$x_{Ir}(t) = 1 - \frac{1}{[1+(r-1)x_{0A1}(t)]^{\frac{1}{r-1}}} \le\ x_{A1}(t) = 1 - exp[-x_{0A1}(t)],\ x_{0A1}(t) = Z_{A1}t^{n_{A1}} \tag{7}$$

where r≥1 is the correction exponent, and the exponent function equals the original Avrami by Eq. (1). As depicted in Fig. 3, where the general term Q(z) designates the crystalline mass fraction (x), the formula $x_{Ir}(t)$ increasingly tends to the original Avrami equation, $x_{A1}(t)$, when the correction exponent, r, tends to 1 (Supplementary materials A2) [31], (8):

$$x_{Ir}(t) \underset{r\to 1}{\to} x_{A1}(t);\ x_{Ir}(t) \sim\ x_{0A1}(t),\ t\to 0 \tag{8}$$

Fig. 3 excellently illustrates that the modified formula, $x_{Ir}(t)$ describes a slower and less complete crystallisation process than the Avrami one, $x_{A1}(t)$, corresponding to numerous experiences reported in the literature [24–28].

The results based on *Concepts II or III* have been proven to be implicit

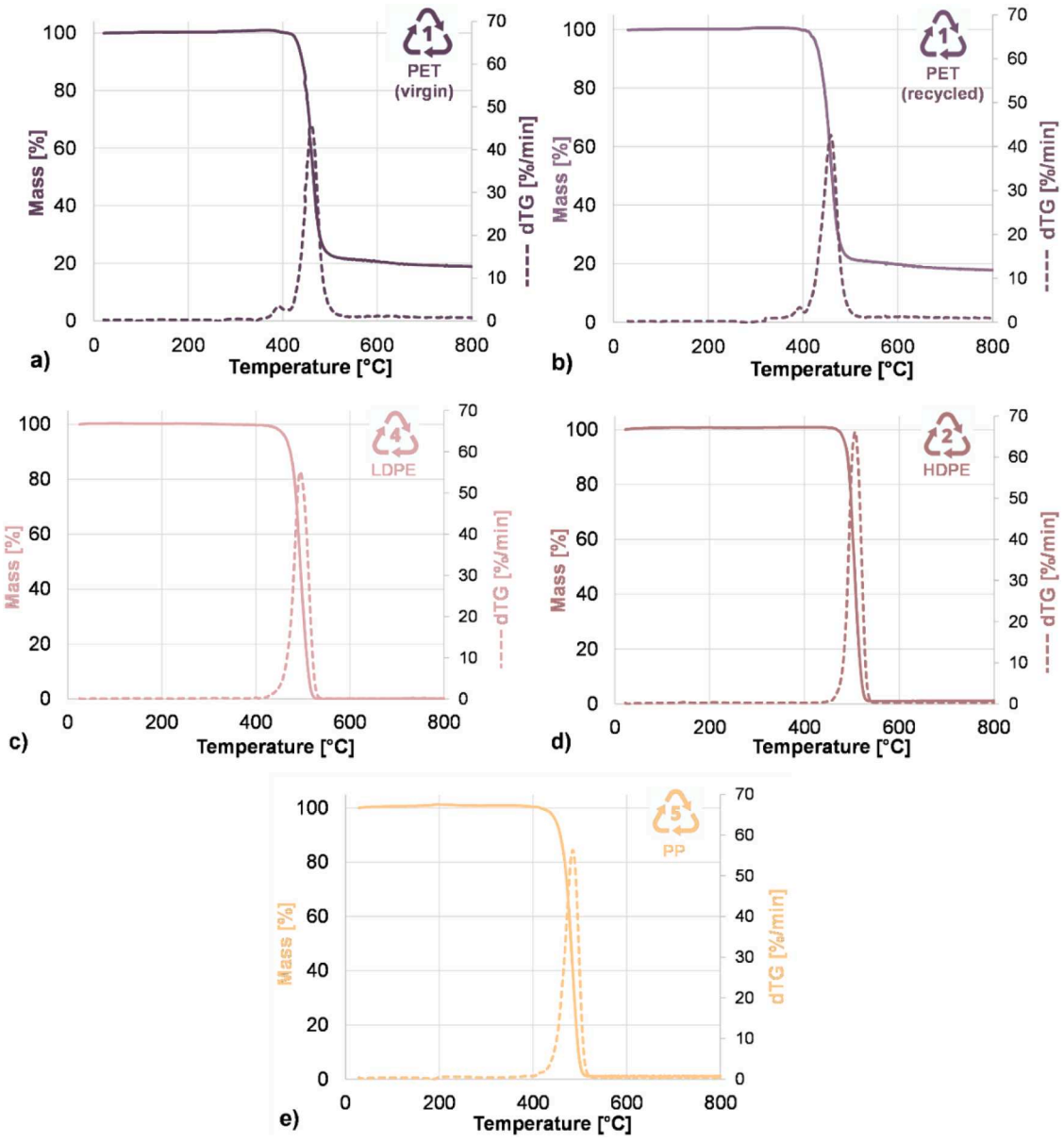

Fig. 5. TGA and DTG curves of the materials tested: vPET (a); rPET (b); LDPE (c); HDPE (d); and PP (e).

Table 3
The decomposition temperatures of the materials tested.

Material	Decomposition		
	T_{DTG0} [°C]	T_{DTGmax} [°C]	T_{DTGf} [°C]
vPET	371	461	533
rPET	363	459	531
LDPE	426	494	533
HDPE	454	507	540
PP	406	485	520

integral equations or the solution of nonlinear differential equations (see Supplementary materials A2); therefore, subsequently, *Concept I* was applied to extend the Avrami formula for both types of nucleation.

2.3. Modified and extended avrami equation for instantaneous and random nuclei

Considering the instantaneous and the random nucleation and the spatial hindrance provides an extended (index *E*) form of the Avrami (index *A*) formula by Eq. (1) (see Supplementary materials A3), (9–10):

$$x_{AE}(t) = 1 - exp[-x_{0AE}(t)] \tag{9}$$

where:

$$x_{0AE}(t) = Z_{A0}t^{n_{A0}} + Z_{A1}t^{n_{A1}} \tag{10}$$

Concept I provided a modified extension of the Avrami formula (MEA2 or Avrami Advanced model), $x_{IEr}(t)$ for both instantaneous and random nuclei where the instantaneous nuclei were incorporated from the Avrami formula by Eq. (1) and the random nuclei from the corrected formula by Eq. (7) (see Supplementary materials A3), Eq. (11):

$$x_{IEr}(t) = 1 - \frac{e^{-Z_{A0}t^{n_{A0}-1}}}{[1+(r-1)Z_{A1}t^{n_{A1}}]^{\frac{1}{r-1}}} \leq x_{AE}(t) = 1 - exp[-x_{0AE}(t)] \tag{11}$$

where n_{A0} and n_{A1} are the Avrami exponents belonging to the instantaneous and random nuclei, respectively. Another approximate extension, $x_{IELr}(t)$, as a kind of lower (subscript *L*) estimation of $x_{IEr}(t)$ (MEA1),

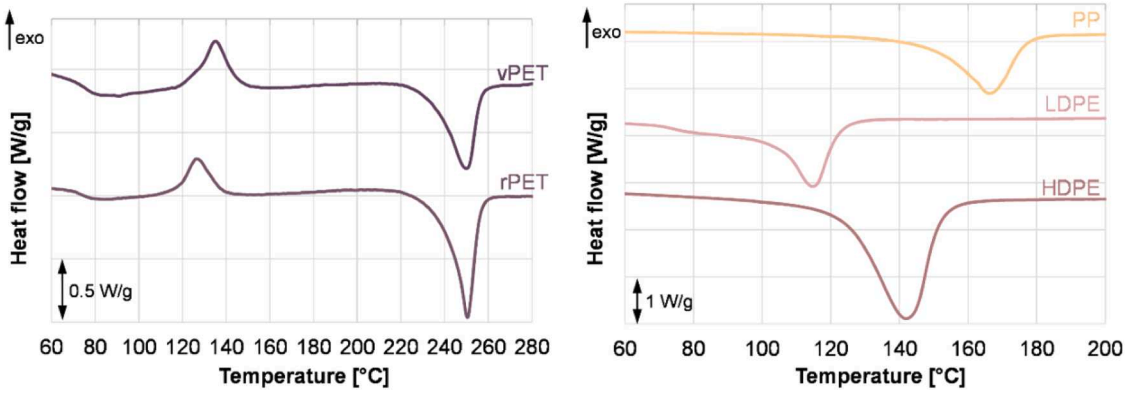

Fig. 6. DSC curves of the materials tested – obtained at the first heating: vPET and rPET (a) and PP, LDPE, and HDPE (b).

Table 4
The transition temperatures of the materials tested determined by DSC (subscript 'o' stands for onset, 'p' for peak, 'f' for final).

Material	Cold crystallisation			Crystal melting		
	$T_{cc,o}$ [°C]	$T_{cc,p}$ [°C]	$T_{cc,f}$ [°C]	$T_{m,o}$ [°C]	$T_{m,p}$ [°C]	$T_{m,f}$ [°C]
vPET	126	135	145	235	250	256
rPET	118	127	138	242	251	256
LDPE	N/A			104	115	123
HDPE	N/A			125	142	152
PP	N/A			150	169	178

for both instantaneous and random nuclei could be obtained by modification based directly and formally on *Concept I* and Eq. (7) as follows (see Supplementary materials A3), (12):

$$x_{IELr}(t) = 1 - \frac{1}{[1+(r-1)x_{0AE}(t)]^{\frac{1}{r-1}}} \le x_{IEr}(t) \le x_{AE}(t) = 1 - exp[-x_{0AE}(t)] \quad (12)$$

Both formulae tend to the Avrami function $x_{AE}(t)$ or the initial asymptote $x_{0AE}(t)$ when the correction exponent r tends 1 or the time (t) tends to 0, respectively, (13):

$$x_{jr}(t) \underset{r\to 1}{\to} x_{AE}(t),\ x_{jr}(t) \sim x_{0AE}(t),\ t\to 0;\ j = IE,\ IEL \quad (13)$$

It is important to clarify that the exponents of the introduced power functions in the modified and extended formulae are integers that are Avrami exponents, consequently the relations to the nucleus dimensions can be understood similarly to those of the original Avrami formula.

Based on the formulae and their relations in Eqs. (11) and (12), the function $x_{IEr}(t)$ can formally be generalized for the ***polymorphic crystallinity*** as follows (14):

$$x_{IEr}(t) = 1 - \frac{e^{-x_{0AE0}(t)}}{[1+(r-1)x_{0AE1}(t)]^{\frac{1}{r-1}}} \quad (14)$$

where the asymptotes for the instantaneous and random nucleation are (15):

$$x_{0AE0}(t) = \sum_{i=1}^{K_0} Z_{A0i} t^{n_{A0i}},\ x_{0AE1}(t) = \sum_{j=1}^{K_1} Z_{A1j} t^{n_{A1j}} \quad (15)$$

Parameters K_0 and K_1 are the numbers of the crystalline system types for the instantaneous and random nucleation, respectively.

2.4. Fraction of instantaneous nuclei and the related crystals

The essential effect of nucleating agents is realized in the increasing number of the instantaneous nuclei. This effect can be characterized by the subsequent numerical properties. On the other hand, if different types of crystals can be found in the polymer, the formulae above enable to plan their fractions.

2.4.1. Ratio of the instantaneous nuclei at the beginning of the crystallisation process

The basis of the following calculations is the facts that the initial asymptote of the crystallisation functions, $x_{jr}(t)$ (1<r<2; j=IE, IEL), according to Eqs. (11) and (12) equals that of the extended Avrami formula, $x_{AE}(t)$, independently of the value of the *correction exponent r*, and the functions $x_{jr}(t)$ tend to the extended Avrami formula if r→1. The *initial asymptote* $x_{0AE}(t)$ by Eq. (11) is a polynomial, the characteristic exponents of which (n_{A0} and n_{A1}) are Avrami exponents. The shape of this, if the developing geometry of the instantaneous and the random nuclei is the same is $n_{A1}=n_{A0}+1$, as follows (16):

$$x_{0AE}(t) = Z_{A0} t^{n_{A0}} + Z_{A1} t^{n_{A0}+1} \quad (16)$$

Hence, the ratio of the Avrami coefficients Z_{A0} and Z_{A1} belonging to the d-dimensional instantaneous and random nucleation given by exponents n_{A0} and $n_{A1}=n_{A0}+1$ is in every case (d=1, $n_{A0}=1$; d=2, $n_{A0}=2$; d=3, $n_{A0}=3$), (17):

$$\frac{Z_{A0}}{Z_{A1}} = \frac{P_0}{\dot{P}_0} =: \tau \quad (17)$$

where τ is the time constant of the nucleus formation which is the duration in which the number of random nuclei formed in a volume unit equals the number of the instantaneous nuclei formed at the beginning of the crystallisation. Consequently, this is a characteristic of the crystallisation process, as well.

The developing geometry is of d-dimensions (d=1, 2, 3) in general, therefore any of the extended formulae is considered the shape of the initial asymptote by Eq. (10) is as follows (18):

$$x_{0AE}(t) = (P_0 + \dot{P}_0 t)\frac{\rho_S}{\rho_L}\pi \begin{cases} \frac{1}{3}\dot{L}_0{}^3 t^3, & d=3 \\ \frac{h}{3}\dot{L}_0{}^2 t^2, & d=2 \\ \frac{A_0}{2}\dot{L}_0{}^1 t^1, & d=1 \end{cases} \quad (18)$$

Eq. (18) is a sum related to the instantaneous and the random nuclei, the part of which in the parenthesis is the same in every case ($n_{A0}+1=n_{A1}$), hence the initial time-depending ratio of the instantaneous (index: i=0) and the random (index: i=1) nuclei, $\phi_{00}(t)$ and $\phi_{01}(t)$, respectively are (19):

$$\phi_{00}(t) = \frac{P_0}{P_0 + \dot{P}_0 t} = \frac{1}{1+\frac{t}{\tau}},\ \phi_{01}(t) = \frac{\dot{P}_0 t}{P_0 + \dot{P}_0 t} = \frac{\frac{t}{\tau}}{1+\frac{t}{\tau}} \quad (19)$$

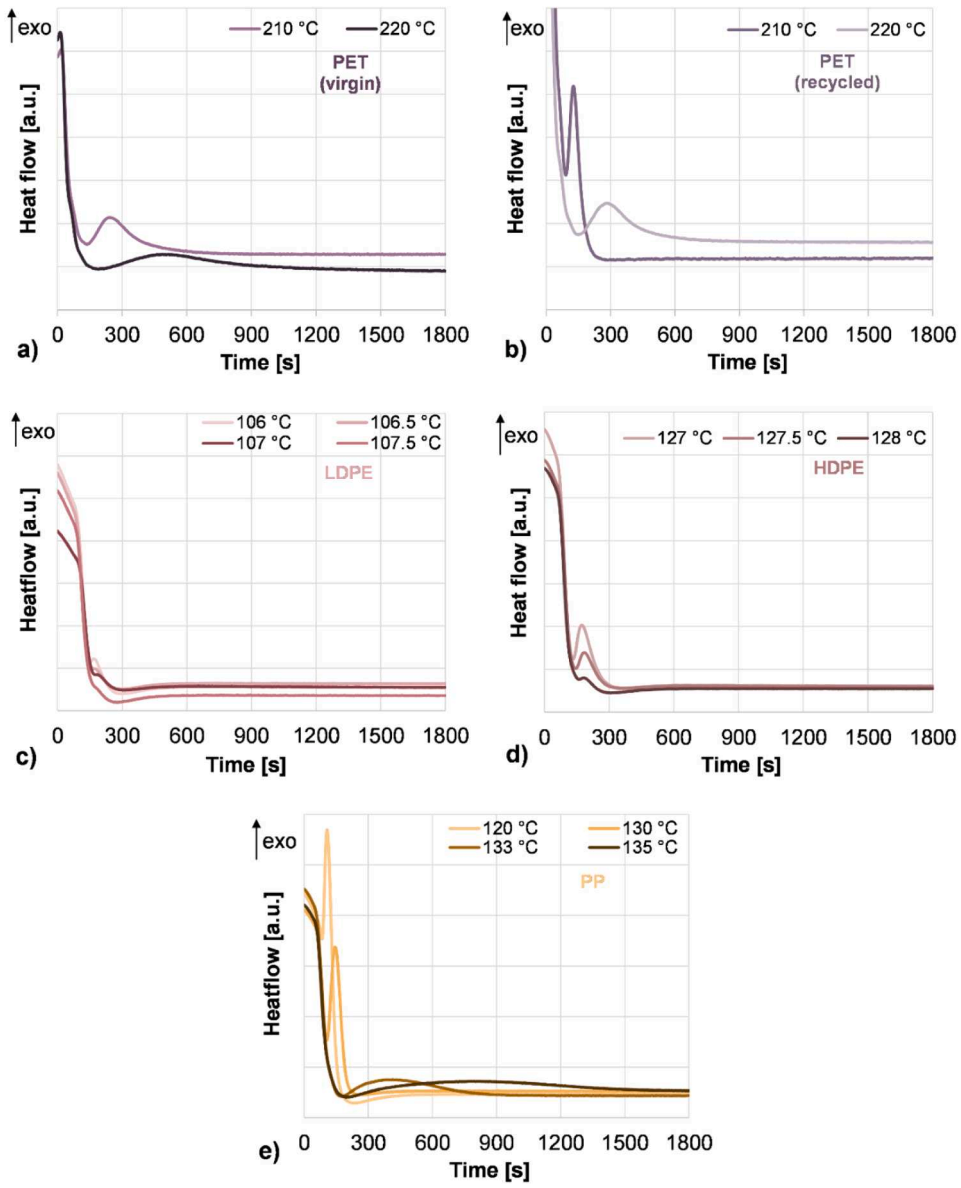

Fig. 7. Isothermal crystallisation curves of vPET (a), rPET (b), LDPE (c), HDPE (d) and PP (e).

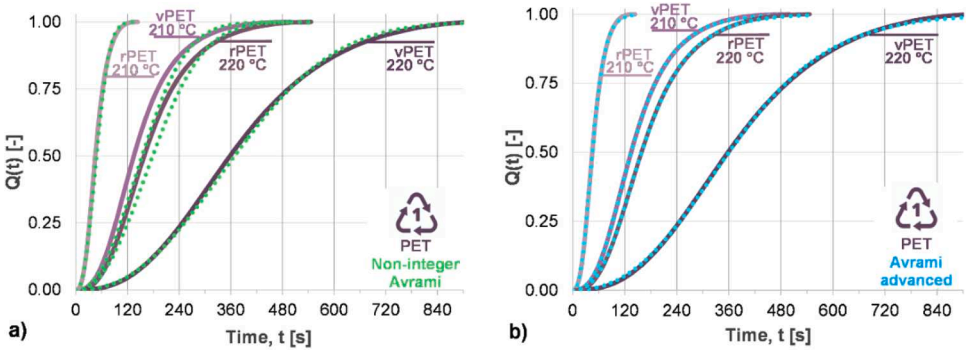

Fig. 8. The measured normalized crystallisation curve of virgin and recycled PET materials at 210 °C and 220 °C and their approximations based on the LogLogLin fitted Avrami formula (a,c) and the nonlinear fitted MEA2 Avrami formula (b,d).

As expected, the ratio $\phi_{0a}(t)$ is 100 % at t=0 and decreases hyperbolically with the time, while the ratio $\phi_{01}(t)$ changes adversely. We obtain the values characterizing the process if we consider the value of Eq. (19) at a properly small time, for example at $t_{0.1}$ ($x(t_{0.1})=0.1$) belonging to the 10 % of the process x(t). In this case, applying this to Eq. (19) we obtain (20):

Table 5
Avrami parameters of the samples (Non-integer model results).

Sample	Avrami – Non-integer model			Avrami		Peak		Crystallisation time and fraction		Lin. trend	Abs. error
	n	B	R^2	Z_A [s^{-n}]	t_A [s]	t^* [s]	t^*/t_A	t_{total} [s]	$x(t_{total})$ [%]	R^2	RMAE%
vPET 210 °C	2.227	−5.030	0.9907	9.33E-6	181.4	237.1	1.307	498.6	25.1	0.9858	10.183
vPET 220 °C	2.325	−6.127	0.9969	7.46E-7	431.6	549.6	1.274	143.6	24.9	0.9993	2.323
rPET 210 °C	2.340	−4.088	0.9979	8.17E-5	55.9	70.9	1.269	948.2	30.0	0.9971	4.819
rPET 220 °C	2.255	−5.236	0.9929	5.81E-6	210.1	272.5	1.297	546.4	29.0	0.9878	9.095
PP 120 °C	2.344	−3.980	0.9740	1.05E-4	49.9	63.3	1.268	155.0	39.0	0.9669	15.878
PP 130 °C	2.670	−4.777	0.9861	1.67E-5	61.5	73.4	1.192	170.0	37.9	0.9849	11.029
PP 133 °C	2.333	−5.899	0.9935	1.26E-6	337.8	429.4	1.271	810.2	37.1	0.9974	3.752
PP 135 °C	2.184	−6.191	0.9939	6.44E-7	684.3	905.9	1.324	1487.4	38.7	0.9977	4.199
LDPE 106 °C	2.143	−3.733	0.9966	1.85E-4	55.2	74.0	1.341	153.8	32.1	0.9981	3.236
LDPE 106.5 °C	2.623	−4.586	0.9933	2.59E-5	56.0	67.3	1.201	133.8	32.8	0.9969	4.180
LDPE 107 °C	2.428	−4.304	0.9871	4.97E-5	59.2	73.6	1.244	142.4	33.5	0.9968	4.274
LDPE 107.5 °C	2.669	−4.610	0.9970	2.46E-5	53.4	63.6	1.192	115.2	33.5	0.9994	1.913
HDPE 127 °C	2.335	−4.500	0.9793	3.16E-5	84.6	107.4	1.270	246.6	62.6	0.9780	12.416
HDPE 127.5 °C	2.225	−4.195	0.9937	6.38E-5	76.9	100.5	1.308	208.4	61.2	0.9932	6.954
HDPE 128 °C	2.502	−4.587	0.9954	2.59E-5	68.1	83.5	1.226	161.8	57.5	0.9975	4.095

Table 6
Parameters obtained by fitting the Advanced Avrami formula.

Sample	Instantaneous nuclei, n_{A0}=2		Random nuclei, n_{A1}=3			Peak	Goodness of fitting MEA2		
	Z_{A0} [s^{-n}]	t_{A0} [s]	r-1	Z_{A1} [s^{-n}]	t_{A1} [s]	t^* [s]	RMSE%	R^2	RMAE%
vPET 210 °C	1.21E-05	287.4	1.240	2.62E-07	156.2	111.2	0.218	1.0000	0.415
vPET 220 °C	1.28E-04	88.3	0.804	5.53E-06	56.6	39.8	0.525	0.9998	1.011
rPET 210 °C	2.76E-06	602.0	0.793	8.19E-09	496.2	322.4	0.376	0.9999	0.595
rPET 220 °C	8.69E-06	339.1	1.158	1.57E-07	185.4	132.6	0.287	0.9999	0.541
PP 120 °C	9.53E-05	102.4	0.6454	1.58E-05	40	30.8	0.2527	0.9999	0.965
PP 130 °C	4.84E-05	143.7	0.3204	5.95E-06	55	44.0	0.1371	1.0000	0.424
PP 133 °C	8.20E-06	349.2	0.0010	1.51E-09	872	246.4	0.3221	0.9999	0.775
PP 135 °C	1.77E-06	752.1	0.0010	2.92E-10	1508	528.2	0.7770	0.9996	1.190
LDPE 106 °C	3.00E-04	57.74	0.85	2.90E-07	151.08	40.60	1.175	0.9981	2.928
LDPE 106.5 °C	1.32E-04	86.90	0.68	4.18E-06	62.05	42.60	1.065	0.9994	1.850
LDPE 107 °C	2.90E-04	58.72	0.85	1.00E-07	215.44	41.40	0.993	0.9993	1.803
LDPE 107.5 °C	1.90E-04	72.55	0.12	3.00E-06	69.34	43.60	0.836	0.9996	1.497
HDPE 127 °C	1.56E-05	253.06	0.9897	3.93E-6	63.36	49.20	1.304	0.9988	2.358
HDPE 127.5 °C	1.65E-04	77.85	0.700	3.00E-7	149.38	54.20	1.1790	0.9989	2.570
HDPE 128 °C	9.91E-05	100.48	0.390	2.10E-6	78.09	53.00	1.0240	0.9993	1.982

$$\phi_{00}(t_{0.1}) = \frac{1}{1+\frac{t_{0.1}}{\tau}},\ \phi_{01}(t_{0.1}) = 1-\phi_{00}(t_{0.1}) = \frac{\frac{t_{0.1}}{\tau}}{1+\frac{t_{0.1}}{\tau}} \tag{20}$$

Based on the value by Eq. (20), the effect of the filling material or the artificial nucleation agent can be assessed. During the crystallisation process, the instantaneous and random nuclei hinder each other in the growing, therefore the separation is not so simple.

2.4.2. Ratio of the crystalline parts developed from instantaneous nuclei at the end of the crystallisation process

Besides the initial ratio of the instantaneous nuclei, $\phi_{00}(t_{0.1})$, the determination of the time-dependent ratio, $\phi_0(t)$, and its steady state value, $\phi_0(\infty)$, of the crystalline parts developed from the instantaneous nuclei and related to the total crystalline mass in the solid polymer may be even more important (see also Supplementary materials A1), (21):

$$\phi_{0,IE}(t) = \frac{x_{IE0}(t)}{x_{IE}(t)} = \frac{1}{x_{IE}(t)}\frac{\rho_S}{\rho_L}P_0\int_0^t (1-x_{IE}(u))dv_0(u)$$
$$= \frac{n_{A0}Z_{A0}}{x_{IE}(t)}\int_0^t (1-x_{IE}(u))u^{n_{A0}-1}du \tag{21}$$

Considering that $x_{IE}(t)\to 1$ when $t\to\infty$, and using the extended Avrami formulae given by the right and left sides of Eqs. (10) and (12), the steady state value, $\phi_0(\infty)$ can be calculated by Eqs. (21)–(24) that can be applied to assessments:

$$\phi_{0,AE}(\infty) = n_{A0}Z_{A0}\int_0^\infty u^{n_{A0}-1}e^{-(Z_{A0}u^{n_{A0}}+Z_{A1}u^{n_{A1}})}du \tag{22}$$

$$\phi_{0,IEL}(\infty) = n_{A0}Z_{A0}\int_0^\infty \frac{u^{n_{A0}-1}}{[1+(r-1)(Z_{A0}u^{n_{A0}}+Z_{A1}u^{n_{A1}})]^{\frac{1}{r-1}}}du \tag{23}$$

$$\phi_{0,IE}(\infty) = n_{A0}Z_{A0}\int_0^\infty \frac{u^{n_{A0}-1}e^{-Z_{A0}u^{n_{A0}}}}{[1+(r-1)Z_{A1}u^{n_{A1}}]^{\frac{1}{r-1}}}du \tag{24}$$

where in general 1<r, and when r→1 formulae (23) and (24) tend to formula (22). Besides, the steady state values by Eqs. (22)–(24) are related to one another by the next inequalities (25):

$$\phi_{0,AE}(\infty) \le \phi_{0,IE}(\infty) \le \phi_{0,IEL}(\infty) \tag{25}$$

Consequently, from fitting Eqs. (11) to the measured isothermal crystallisation process, we can assess the values of all the related parameters with which $\phi_{0,IE}(\infty)$ can be calculated.

2.5. Fitting the model

To the measured crystallisation curves basically two types of

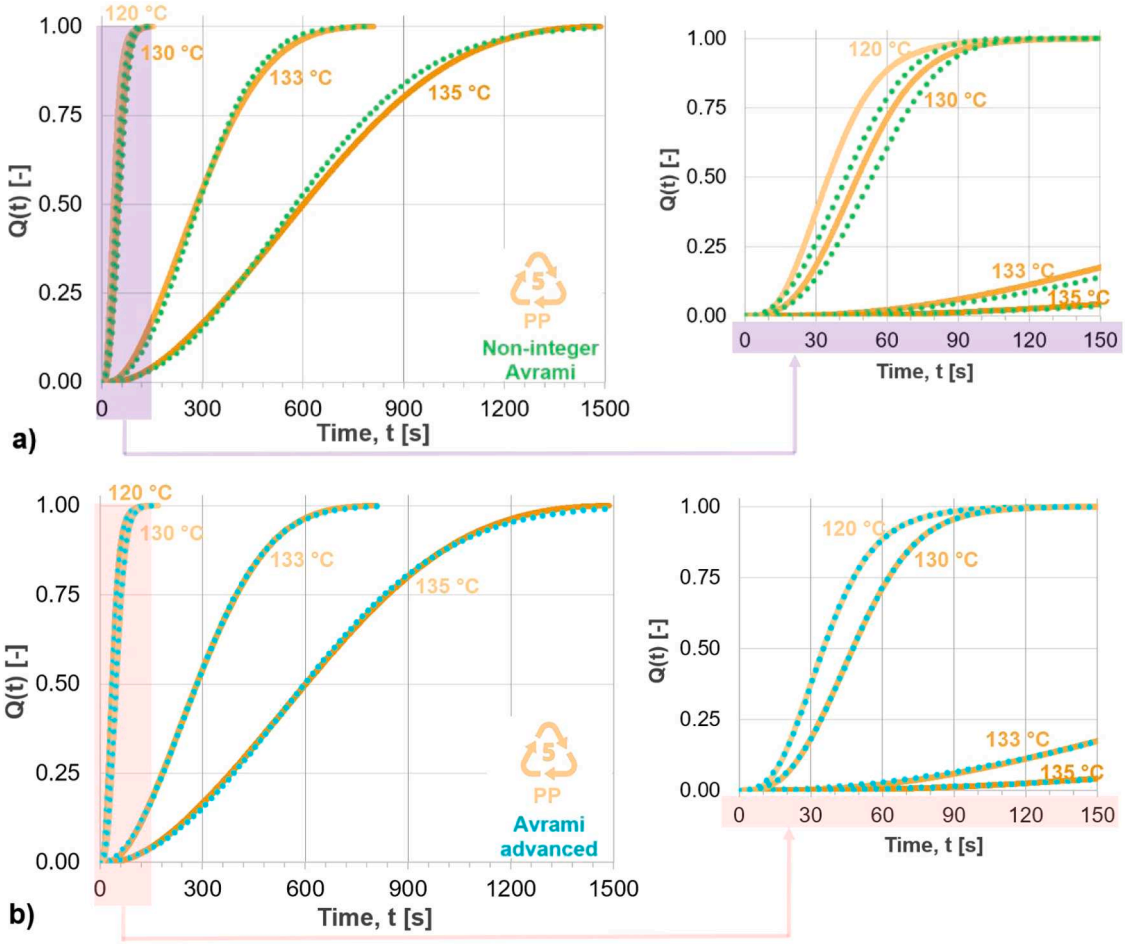

Fig. 9. The measured normalized isothermal crystallisation curves of PP and their approximations based on the Non-integer Avrami formula (a) and the Advanced Avrami formula (b).

relationships were fitted:

#1. Fitting the classical Avrami formula by logarithmic linearizing of Eq. (1) (**Non-integer Avrami formula**) as usual applying Eqs. (5) and (6) (see Chapter 4.2.) The fitting provided the exponent *n* as a real number.
#2. Fitting the non-linear modified and extended Avrami formula (**Advanced Avrami formula**) elaborated in this paper, given by Eqs. (10) and (11), that is valid for both the instantaneous and the random nuclei, using MS Excel Solver extension (see Chapter 4.2.) In these cases, the exponents, n_{A0} and n_{A1}, were integer numbers corresponding to the original understanding of Avrami *et al.*

The goodness of fitting was characterized by the relative maximum absolute error (RMAE), (26), the relative mean squared error (RMSE), (27) and the related determination coefficient (R^2). The latter was obtained from calculating the homogeneous linear trend between the measured and the model curves.

$$RMAE = \frac{\max\limits_{1\le i\le N}|x_{model}(t_i) - x_{measured}(t_i)|}{\max\limits_{1\le i\le N}|x_{measured}(t_i)|} \tag{26}$$

$$RMSE = \frac{\sqrt{\frac{1}{N}\sum_{i=1}^{N}[x_{model}(t_i) - x_{measured}(t_i)]^2}}{\max\limits_{1\le i\le N}|x_{measured}(t_i)|} \le RMAE \tag{27}$$

The maximum of the measured normalized crystallisation curve (it is denoted by Q(t) in the related diagrams) was 1 at its end in every case.

3. Materials and methods

3.1. Materials tested

To analyse the crystallisation process of thermoplastic polymers and determine the accuracy of the model, we carried out isothermal differential scanning calorimetry (DSC) measurements on PET, PP, LDPE and HDPE granules.

The PET materials tested were a virgin (NeoPET 80 (Neo Group, Lithuania)) and a recycled (Jász-Plasztik Kft., Hungary) material that are abbreviated as vPET and rPET, respectively. The intrinsic viscosity ([η]) of vPET was 0.80±0.02 dl/g and the weight-average molecular weight (M_w) measured by GPC was 27,400 g/mol. RPET had an [η] value of 0.56±0.03 dl/g and its M_w was 16,900 g/mol [32]. The recycled material was the grounds of the plastic which accumulates during food packaging production.

The PP tested was a Tipplen H-681F polypropylene homopolymer produced by MOL Petrolkémia Zrt., Hungary. It is a grade recommended for extrusion.

The PE materials tested were a Tipolen FA 244–51 low density polyethylene copolymer and a Tipelin 1100 J high density unimodal polyethylene copolymer produced by MOL Petrolkémia Zrt., Hungary.

3.2. Thermal characterization methods

Thermogravimetry (TGA) measurements were carried out on a

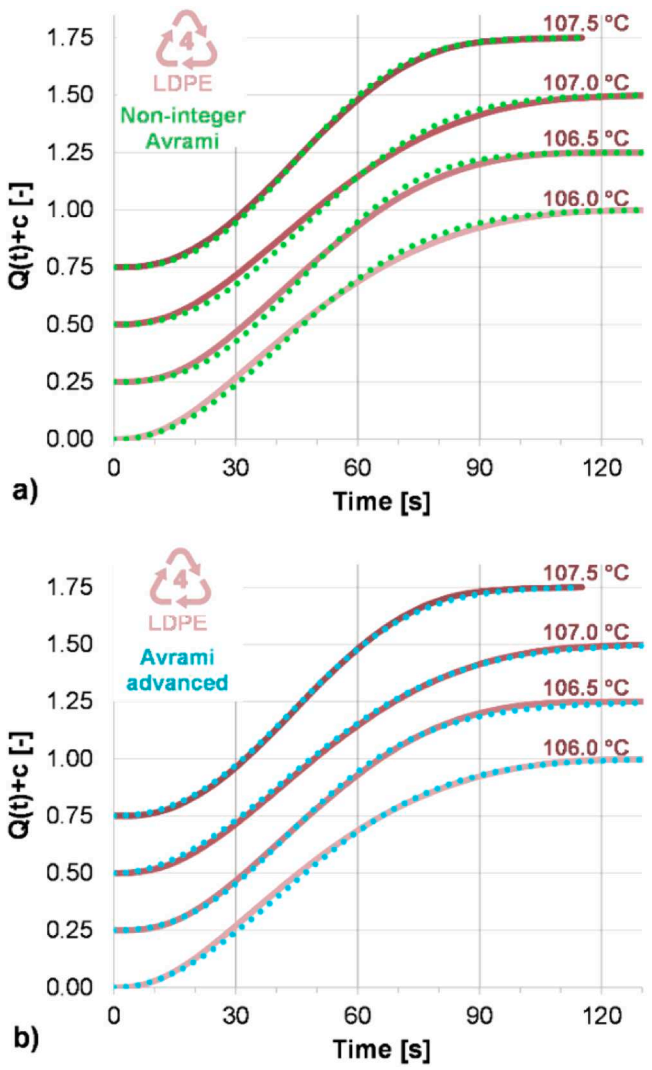

Fig. 10. The measured normalized isothermal crystallisation curves of LDPE and their approximations based on the Non-integer Avrami formula (a) and the nonlinear fitted Advanced Avrami formula (b).

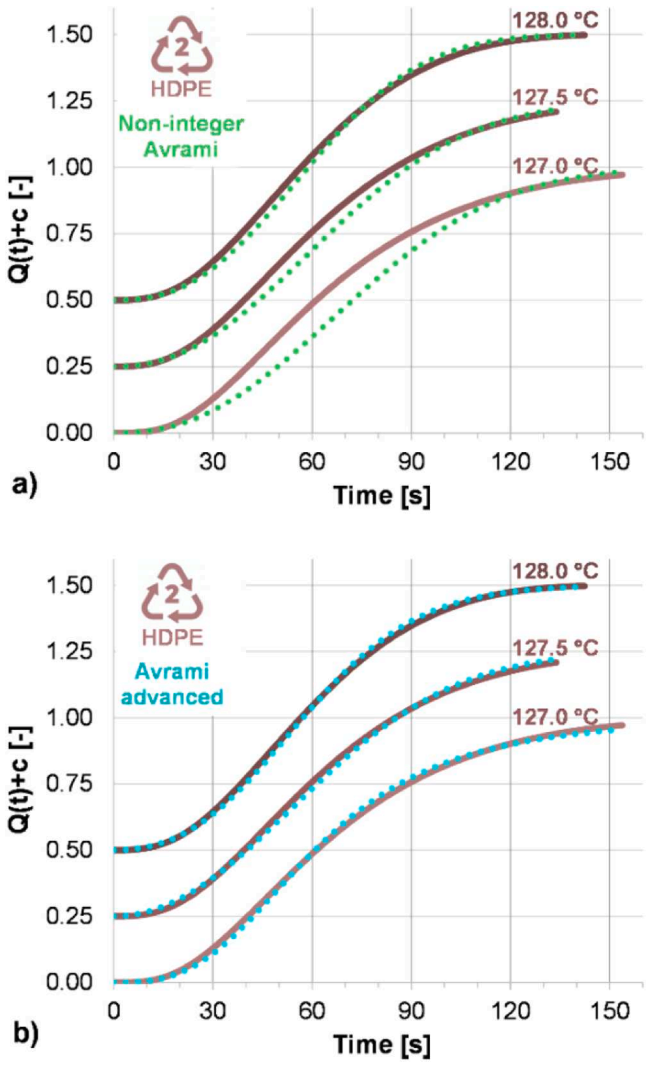

Fig. 11. The measured normalized isothermal crystallisation curves of LDPE and their approximations based on the Non-integer fitted Avrami formula (a) and the nonlinear fitted Advanced Avrami formula (b).

Setaram (LabSys EVO; Caluire-et-Cuire, France) type device in a nitrogen gas purge of 50 ml/min. The characteristics of the materials were measured from room temperature (~20 °C) up to 800 °C with a heating rate of 20 K/min. The derivative thermogravimetric (DTG) curve was also determined.

The DSC measurements of 5–10 mg samples were performed on a Setaram (DSC 131 EVO; Caluire-et-Cuire, France) device according to a heat-cool-isothermal crystallisation-cool-heat cycle in a nitrogen atmosphere with a nitrogen purge flow rate of 50 ml/min. The temperature scale of the DSC was calibrated from the melting point of high purity metals (99.99 %): lead, tin and indium. The detailed thermal sequence was as follows (Fig. 4 and Table 2):

(1) Heating from ambient temperature, T_0, above the T_m melting temperature, T_1, with a β_1=20 K/min heating rate;
(2) Equilibrating at temperature T_1 for time t_1=5 min;
(3) Cooling to the crystallisation temperature T_2=T_{cr} with a β_2=50 K/min cooling rate;
(4) Isothermal crystallizing at temperature T_{cr} for t_2=30 min,
(5) Cooling to ambient temperature T_0 with a β_0 = β_2 =50 K/min cooling rate,
(6) Annealing at ambient temperature T_0 for t_3=5 min
(7) Heating from temperature T_0 to melting temperature T_1 with a β_1=20 K/min heating rate;
(8) Free cooling to ambient temperature T_0.

The initial rise in the curve corresponds to the thermal stabilization of the equipment, as the sample was rapidly cooled at 50 K/min from T_1 down to the crystallization temperature (T_2 = T_{cr}), and the isothermal run was immediately started. The induction time (that in this case includes the stabilization time) has been named t_0 and was deduced from time t (i.e., the time at which the experiment was started).

The crystallisation temperature was T_{cr}=210 °C and 220 °C for the virgin (vPET) and the recycled PET (rPET). In the case of PP, we applied four different values between 120 °C and 135 °C to test at which temperature the crystallisation peak could be evaluated the best. According to the results, the heat-flow peak fell on the initial transient range at 120 °C and 130 °C. At 133 °C and 135 °C, we obtained a "very good" and „satisfactory" peak, respectively.

In the case of HDPE and LDPE materials, the crystallization temperature steps were only 0.5 °C, because a measurable crystallization exothermic peak was only observed in a narrow temperature range. Below the applied minimum T_{cr} incomplete DSC traces were observed; while above the applied maximum T_{cr} the peak was too flat, resulting in an insufficient signal-to-noise ratio.

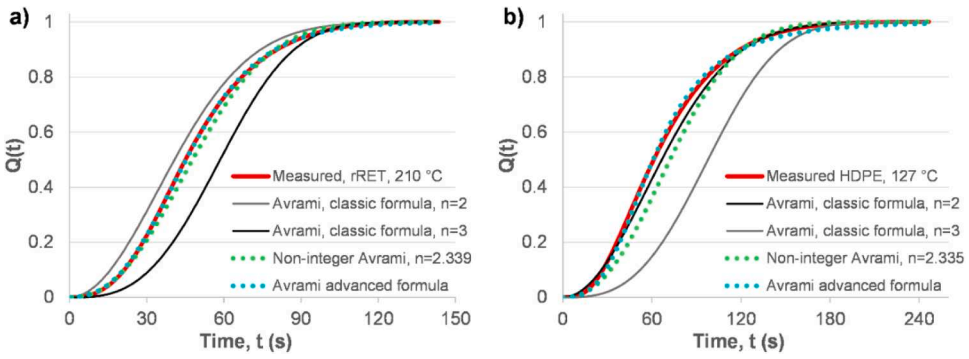

Fig. 12. The measured crystallisation curves of rPET at 210 °C (a) and HDPE at 127 °C (b) and their approximations based on the classic Avrami formula, the Non-integer Avrami formula and the Avrami advanced formula.

Table 7
Determination coefficients obtained by fitting linear trend between the approximate and the measured crystallisation curves in Fig. 11.

Sample code	Fitted approximate curves			
	Avrami (n = 2) R^2	Avrami (n = 3) R^2	Non-integer Avrami R^2	Advanced Avrami R^2
rPET 210 °C	0.9891	0.9167	0.9971	0.9998
HDPE 127 °C	0.9955	0.7486	0.9780	0.9988

The crystallinity of the materials was calculated from the heating after the isothermal crystallisation. The following equation was applied for the computation [33], (28):

$$x_{total} = \frac{\Delta H_m}{\Delta H_m^{100}} \cdot 100\% \quad (28)$$

where x_{total} is the crystallinity after crystallisation [%], ΔH_m is the melting enthalpy of the sample [J/g] and ΔH_{m100} is the heat of fusion [J/g]. We took the value of ΔH_{m100} from the literature as 140 J/g for PET [34], 293 J/g for LDPE and HDPE [35] and 207 J/g for PP [33].

Based on the TGA curves (see Fig. 5), we established that the polymer materials used do not degrade at the chosen isothermal crystallisation temperatures (Table 2).

Subsequently, the results of the isothermal crystallisation measurements performed on the PET, PP and PE polymer samples and the applicability of the Avrami formula, and its modified versions were analysed in the description of the crystallisation process.

4. Results and discussion

4.1. Thermal data

Fig. 5 shows the TGA/DTG curves of the materials tested. We obtained the decomposition temperatures belonging to the maximum rate of mass decrease from the inflexion point of the derivative curves. We tabulated the results obtained this way in Table 3.

The transition temperatures denoted as $T_{x,o}$ and $T_{x,f}$ are the onset (lower) and final (upper) temperatures of the transition range respectively, which can be defined as the inflection tangents of the vertex and the intersection points of the baseline. T_{DTG} belongs to the mass reduction by decomposition and T_{DTGmax} denotes the temperature to peak.

Based on the results, we conclude that no significant degradation can be expected throughout the crystallisation process. Heat treatment for thermal history elimination (at T_1) took place >40 K below the T_{DTG0} temperature, under which there is no degradation, and >140 K below the T_{DTGmax} temperature in all cases. No decomposition took place at the melting temperatures hence the temperature for the isothermal crystallisation (T_2) can be freely chosen below those values.

We present the DSC results in Fig. 6 for all the materials tested and the results are summarized in Table 4. In this case, $T_{cc,p}$ and $T_{m,p}$ signify the cold crystallisation and the melting peaks, respectively. The subscript *o* and *f* again refer to the onset and final temperatures, respectively.

In the case of both PET materials, cold crystallisation took place between 110 °C and 150 °C, which is a common phenomenon for PET materials since they have slow crystallisation kinetics. The spherulite growth rate is very small for PET [36]. Hence, short-time isothermal crystallisation or fast cooling had led to incomplete crystallisation prior to the tests.

4.2. Results of the model fitting

On the vertical axis of the diagrams showing the measured crystallization process and the result of fitting the modified and extended formula, the simple term Q(t) denotes the normalized crystal mass fraction at time *t* in general. Some examples of fitting the classical Avrami formula in the double logarithmic coordinate system according to Eq. (5) can be seen in the Supplementary materials.

4.2.1. Model fitting for pet materials, the effect of recycling

The heat flow curves of the materials tested are presented in Fig. 7. The different isotherms led to different crystallization characteristics and there is also a huge difference between the behaviour of the different materials.

The results on crystallinity and the fitted curves are presented in Fig. 8. In the diagrams, the *Non-integer Avrami* and the *Avrami advanced* (modified and extended Avrami) indicate the methods of fitting #1 and #2, respectively. Note that rPET exhibited a faster crystallisation at the same temperatures that is related to degradation and smaller molecular mass.

The recycled material probably had a smaller molecular mass which needs smaller energy for chain folding and packing. This results in a faster crystallisation kinetics at a given temperature. That is also in line with the fact that cold crystallisation of the rPET took place at a lower temperature determined by DSC (Fig. 6 and Table 4).

The degree of crystallinity was 25 % for vPET and 30 % for rPET, which was not influenced by the crystallisation temperature (210 vs. 220 °C). The crystallinity measured at the end of the isotherm crystallisation and the parameters obtained from fitting Equations (5) (Non-integer Avrami formula) and Eq. (11) (Avrami advanced formula), respectively, for the vPET and rPET samples can be found in Tables 5 and 6 in Chapter 4.3.

4.2.2. Model fitting for PP materials, the effect of temperature

Fig. 9 shows the measured and fitted curves (LogLogLin and MEA2)

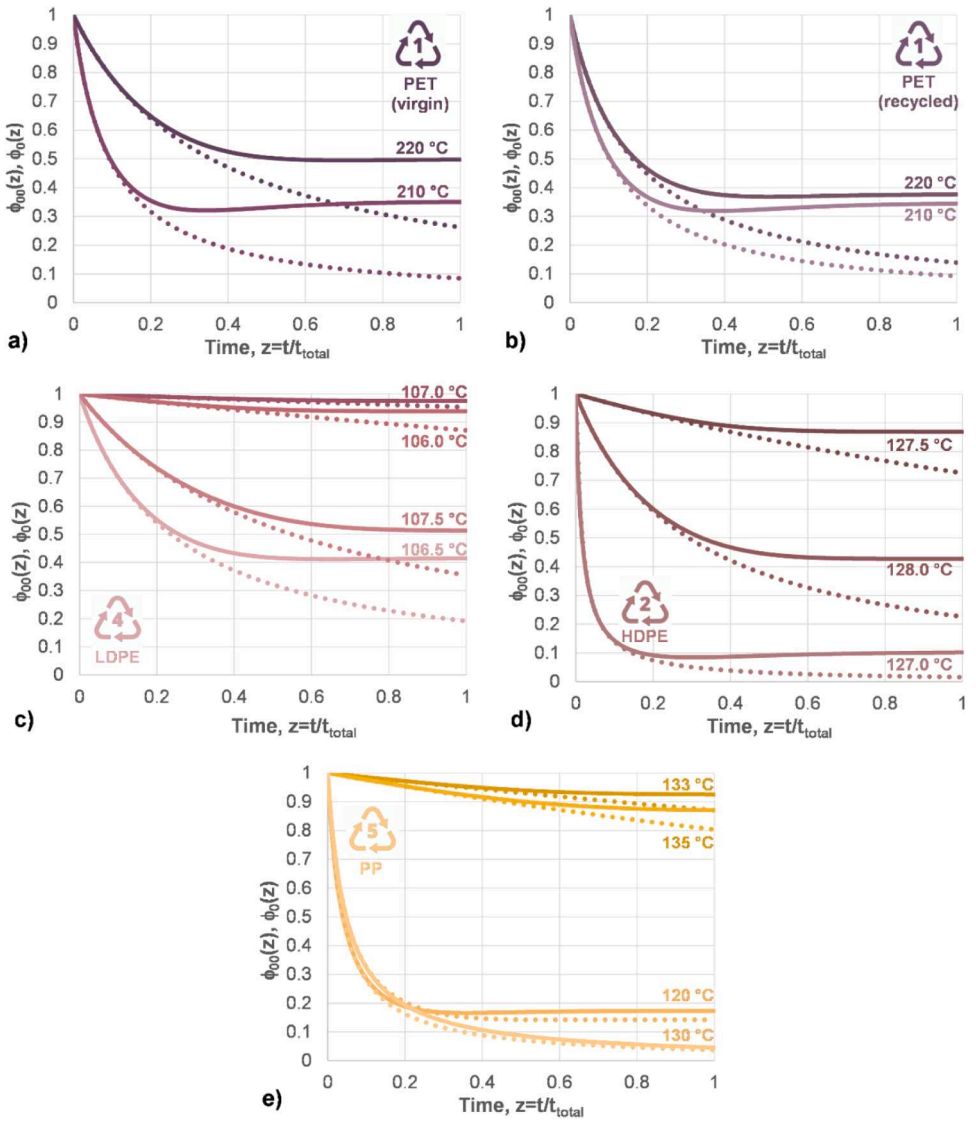

Fig. 13. The I-nucleus-based initial and final crystallinity vs. time for the virgin PET (a), recycled PET (b), LDPE (c), HDPE (d) and PP (e) samples. The continuous line represents the I-nuclei based relative crystalline fraction $\phi_0(z)$, while the dashed line shows the initial ratio of the I-nuclei ($\phi_{00}(z)$).

Table 8
Properties of the nucleus formation and the crystal growing of the samples.

Sample	Inst. nuclei, $n_{A0}=2$		Random nuclei, $n_{A1}=3$			Nucleation			
	Z_{A0} [s^{-n}]	t_{A0} [s]	r-1	Z_{A1} [s^{-n}]	t_{A1} [s]	τ [s]	$t_{0.1}$ [s]	τ /$t_{0.1}$ [-]	ϕ_{00} [%]
vPET 210 °C	1.21E-5	287.38	1.240	2.62E-7	156.23	46.18	62.4	0.740	42.53
vPET 220 °C	1.28E-4	88.32	0.804	5.53E-6	56.56	23.20	21.4	1.084	52.02
rPET 210 °C	2.76E-6	602.01	0.793	8.19E-9	496.19	337.08	165.0	2.043	67.14
rPET 220 °C	8.69E-6	339.13	1.158	1.57E-7	185.45	55.45	74.0	0.749	42.84
PP 120 °C	9.53E-5	102.42	0.645	1.58E-5	39.8	6.02	17.4	0.346	25.69
PP 130 °C	4.84E-5	143.75	0.320	5.95E-6	55.2	8.13	23.8	0.342	25.46
PP 133 °C	8.20E-6	349.20	0.001	1.51E-9	872.1	5439.9	113.8	47.802	97.95
PP 135 °C	1.77E-6	752.06	0.001	2.9E-10	1508.1	6064.7	228.2	26.576	96.37
LDPE 106 °C	3.00E-4	57.74	0.85	2.90E-7	151.08	1034.5	17.8	58.12	98.31
LDPE 106.5 °C	1.32E-4	86.90	0.68	4.18E-6	62.05	31.6	21.2	1.49	59.88
LDPE 107 °C	2.90E-4	58.72	0.85	1.00E-7	215.44	2900.0	20.8	139.42	99.29
LDPE 107.5 °C	1.90E-4	72.55	0.12	3.0E-6	69.34	63.3	21.4	2.96	74.74
HDPE 127 °C	1.56E-5	253.06	0.990	3.93E-6	63.36	3.97	27	0.147	12.82
HDPE 127.5 °C	1.65E-4	77.85	0.700	3.00E-7	149.38	550.00	26	21.154	95.49
HDPE 128 °C	9.91E-5	100.48	0.390	2.10E-6	78.09	47.17	25.8	1.828	64.64

Table 9
Properties of the nucleus formation and the crystal growing of the samples.

Sample	Crystallisation		I-nucleus formation			I-crystallinity		
	t_{total} [s]	$t_{0.1}$ [s]	ϕ_{00}_%	t_{total}/ϕ	$t_{0.1}/t_{total}$	ϕ_0_%	ϕ_0/ϕ_{00}_%	X_0_%
vPET 210 °C	498.6	62.4	42.53	10.80	0.13	34.96	82.19	8.77
vPET 220 °C	143.6	21.4	52.02	6.19	0.15	37.49	72.08	9.34
rPET 210 °C	948.2	165.0	67.14	2.81	0.17	49.38	73.54	14.81
rPET 220 °C	546.4	74.0	42.84	9.85	0.14	34.27	80.01	9.94
PP 120 °C	155.0	17.4	25.69	25.76	0.11	17.30	67.32	6.75
PP 130 °C	170.0	23.8	25.46	20.91	0.14	14.22	55.85	5.39
PP 133 °C	810.2	113.8	97.95	0.15	0.14	92.35	94.28	34.26
PP 135 °C	1487.4	228.2	96.37	0.25	0.15	86.39	89.64	33.43
LDPE 106 °C	153.8	17.8	98.31	0.15	0.12	11.57	11.77	3.72
LDPE 106.5 °C	170.0	23.8	59.88	20.91	0.14	41.27	68.92	13.54
LDPE 107 °C	810.2	113.8	97.95	0.15	0.14	97.30	99.34	32.60
LDPE 107.5 °C	1487.4	228.2	96.37	0.25	0.15	51.23	53.15	17.16
HDPE 127 °C	246.6	27	12.82	62.09	0.11	10.13	78.99	6.34
HDPE 127.5 °C	208.4	26.0	95.49	0.38	0.12	86.86	90.97	53.16
HDPE 128 °C	161.8	25.8	64.64	0.15	0.14	42.66	66.00	24.53

of the isothermal crystallisation process of the PP sample for temperatures 120 °C, 130 °C, 133 °C, and 135 °C. Since the crystallisation kinetics are greatly influenced by temperature, the results are presented at different time scales.

Note that the figures present normalized values. The final degree of crystallinity slightly varies and is between 37 and 39 % depending on the crystallisation temperature. The crystallinity measured at the end of the isotherm crystallisation and the parameters obtained from fitting Equations (5) (Non-integer Avrami model) and Eq. (11) (Advanced Avrami model), respectively, for the PP samples can be found in Tables 5 and 6 in Chapter 4.3.

4.2.3. *Model fitting for LDPE and HDPE materials, the effect of temperature*

The measured and fitted curves (Non-integer and Advanced Avrami models) of the isothermal crystallisation process of the LDPE sample at 106 °C, 106.5 °C, 107 °C, and 107.5 °C are presented in Fig. 10. For a better visualization of the slight effects of temperature, the crystallisation curves are shifted vertically by a constant *c* which was 0.25; 0.5; and 0.75, respectively. Due to the use of smaller crystallization temperature steps, the characteristics of the curves do not differ as strongly as for PET or PP.

Fig. 11 present the measured and the fitted Non-integer and Advanced Avrami model curves of the isothermal crystallisation process of the HDPE sample at 127 °C, 127.5 °C and 128 °C, as well. Again, the latter two curves were shifted vertically by a constant of 0.25 and 0.5 to present the measurements and fitting clearly.

Subsequently, the final crystallinity% and the fitted parameters can be found in Chapter 4.3.

4.3. *Summary and discussion of the results of the measurements and the fittings*

Table 5 contains the crystallinity measured at the end of the isotherm crystallisation and the Avrami parameters obtained in the traditional way from fitting Eq. (5) (Non-integer Avrami) for the PET, PP, and PE samples.

The final crystallinity%, $x(t_{total})$ does not depend on the crystallisation temperature significantly for the PET materials, but it proved itself to be larger by about 5 % for the RPET, which may be attributed to the degradation caused by recycling. Shorter molecules with a smaller M_w tend to crystallise better. That is because the molecule chains are more mobile, and only a smaller number of entanglements – hindering the crystallisation process – exist between them. The crystallinity of the PP samples ranges between 37 % and 39 % as a function of the temperature; however, no significant trend can be observed. Similar to those for the PP, the crystallinity of LDPE versus temperature values do not show any significant trends. Unlike the data for PP and LDPE, the temperature and crystallinity values for the HDPE suggest a decreasing relation.

The most important fact in Table 5 is that the fitted exponent, *n*, is not an integer, but in every case, falls in between two integers, 2 and 3, that are Avrami exponents. The other remarkable fact is that the Avrami time constant, t_A, is smaller than t^* ($t_A<t^*$) belonging to the inflection point of the crystallisation curve indicating the peak of the crystallisation rate but their ratio is about 1.3 in every case. The total crystallisation time, t_{total}, decreases with increasing temperature except for the PP. The peak time, t^*, increases with the temperature in case of PET and PP, while decreases for the HDPE and this relation is changing for the LDPE.

The determination coefficient (R^2) (Lin. trend: direct linear trend between the measured and model data with intercept =0) in Table 5 was used to check the goodness of fitting in the original linear scaled coordinate system. In the case of PET, it is smaller at 210 °C while larger at 220 °C than that provided by the LogLogLin (non-integer) fitting. This means that the LogLogLin (non-integer) trend relation is weaker in the former case and stronger in the latter case than the Lin. trend one. As for PP, the coefficient R^2 of both types gradually increases with the crystallisation time (T_{cr}), while those for the Lin. trends are larger. All that means that the LogLogLin trend relation is weaker than the Lin. trend one. However, in the case of the LDPE and HDPE, the coefficient R^2 of both types does not change gradually with the crystallisation temperature (T_{cr}). Considering the PE samples, the determination coefficient for the Lin. trends is larger than that of the Lin. trends in every case except for HDPE 127 °C and 127.5 °C, but the deviations related to the Lin. data are −0.0013 and −0.0005, while in the other cases they are between +0.0015 and +0.0097.

The parameters of fitting of the modified and extended Avrami formula (Advanced Avrami model) that we developed and given by Eq. (11) can be found in Table 6. The Avrami exponents used in the calculations were $n_{A0}=2$ and $n_{A1}=3$ in every case.

The fitted data in Table 6 show more identifiable relations and trends than those in Table 5, which may indicate a better relation of the extended Avrami formula (Avrami advanced formula) to the material behaviour. First of all, according to Table 1 and the Avrami exponents $n_{A0}=2$, $n_{A1}=3$ in Table 6, both the instantaneous and the random nucleation provide disc-like (2D) growing for all the materials tested. The correction exponent, r, is close to 0 just in cases of PP 133 °C and PP 135 °C meaning that the random nucleation is approximately of Avrami type in contrast to the other cases. For another example, in contrast to Table 5, both Avrami time constants, t_{A0} and t_{A1}, are larger than the peak time t^* corresponding to the inequalities $t^*<t_{A1}<t_{A0}$ for every material. On the other hand, the peak time, t^*, in Table 6 for the PET samples

follows the variation of the crystallisation time, total, while that in Table 5 does not.

Based on all the modelling results we presented and the values of the goodness of fitting in Tables 5 and 6, one can establish that the modified and extended Avrami formula (Advanced Avrami model) by Eq. (11) provided much more accurate fitting than the original Avrami formula (LogLogLin) by Eq. (1). In the latter case, in general, the largest error in fitting could be observed in the middle part of the crystallisation curves like in Fig. 8.a and 9.a or 10.a and 11.a.

Fig. 12 shows two examples to compare the measured curve to the fitted ones where, besides the Non-integer and the Advanced Avrami types, the Avrami curves fitted with prescribed exponents $n = 2$ and $n = 3$ (LogLin) can also be seen. The Non-integer model with exponent between 2 and 3 gives a fair fitting; however, the Advanced Avrami model curve provides better fitting (see Table 7) and important information about the instantaneous and random nucleation geometry. As expected, the LogLogLin curve (non-integer Avrami, $n \approx 2.3$) goes between the two classic Avrami LogLin curves ($n = 2$; $n = 3$), however the measured crystallisation curve may protrude from between them because of its special shape (Fig. 12.b).

As presented in Fig. 12 and in Table 7, the models developed in this paper, and especially the Advanced Avrami model describe the crystallisation process of polymers much better than the classic Avrami formula.

The various data obtained from the fittings in Tables 5 and 6 demonstrate the possibility of determining and defining different numerical properties to characterize and analyse the nucleation and the crystallisation processes and the crystalline structure of the material tested.

4.4. Crystallisation parameter analysis based on the fitted equation

In Fig. 13, the initial ratio of the I-nuclei and the I-nuclei based relative crystalline fraction $\phi_0(z)$ within the crystallinity can be seen together.

The initial ratio of the I-nuclei $\phi_{00}(z)$ (see the dashed lines) and the I-nuclei based relative crystalline fraction $\phi_0(z)$ within the crystallinity – shortly final I-ratio –

(see the solid lines) were calculated by Eqs. (19) and (21), respectively, versus the normalized crystallisation time $z = t/t_{total}$ can be seen together. The first index 0 of ϕ_{00} is for the instantaneous (I) nuclei in the Avrami constants Z_{Ai} and n_{Ai} ($i = 0$), while the second index 0 indicates the initial part of the crystallisation process where the nucleation takes place.

The diagrams visualize the facts that the curves of the I-nucleus ratio are the asymptote of the I-crystal fraction curves and highlight their different variation with time. The former ones are strictly decreasing, while the latter tend to a kind of equilibrium in growing of the instantaneous and random-nuclei-based crystals, which can be attributed to the effect of the random-nucleation-based crystallisation.

4.4.1. Fraction of the instantaneous nuclei

Table 8 shows the time properties of the crystallisation process and the instantaneous nucleus

(Inst. or I-nucleus) formation of the PET, PP, and PE samples, where $\phi_{00\_}=\phi_{00}(t_{0.1})$ was calculated by using Eq. (19).

As an effect of the additional random nucleation, the initial ratio of the instantaneous nuclei decreases with time. The sudden decrease can be observed at lower temperatures for the PP and HDPE, indicating a rapid random nucleation. In the case of the PET and PP materials, the initial ratio of the I-nuclei increases with temperature, including a jump-like change for the PP, above 130 °C. Contrary to the former behaviour, the initial I-nucleus ratio vs. temperature relation shows irregular changing with increasing temperature.

4.4.2. Fraction of crystals developed from instantaneous nuclei

Table 9 contains, and Fig. 13 depicts the relative fraction of the crystals developed from the instantaneous nuclei (see I-crystals) where $\phi_0(z)$ ($z=t/t_{total}$) is the I-crystal fraction within the crystalline parts and calculated by Eq. (21).

The relative value of the I-crystal fraction at the end of the crystallisation process within the crystallinity was estimated by Eq. (29) as follows:

$$\phi_{0\_}\%=\phi_0(1)\approx\phi_{0,IE}(\infty) \tag{29}$$

and its relative value related to the initial I-nucleus ratio is $\phi_{0\_}/\phi_{00\_}\%$. The absolute value of the I-crystallinity is calculated as $X_{0\_}\%=\phi_{0\_}\%\cdot X\_\%/100$ (Table 9) where X_% is the absolute crystallinity measured at the end of the isothermal crystallisation process.

In each case in Fig. 13, relating to the initial state, the I-nucleus based crystal fraction decreases tending to a steady state, however, some of the curves measured at lower temperatures have a week minimum that may be attributed to the most intense random nucleation. This interesting phenomenon should be examined with additional experiments. In most cases, the steady state is reached at the half of the total crystallisation time. This phenomenon may be of importance when planning rapid manufacturing technology like extrusion or injection moulding.

5. Conclusions

Corresponding to the objectives, we developed novel formulae based on the classic Avrami equation. The model we constructed describes the crystallisation process significantly better, and besides that, the model (see Eq. (11)) is simple.

This model we call the “Advanced Avrami formula” was proposed to describe the crystallisation process of polymers including both the instantaneous and the random nucleation. The integer Avrami-exponents in the formula enable us to identify the geometry type of the instantaneous and random nuclei, according to Table 1.

Considering both the instantaneous and the random nucleation and the related crystal development makes the analysis of the effect of the artificial nucleating agents, fillers, and reinforcements possible.

In this paper, additional formulae were introduced to numerically assess the fraction of the instantaneous nuclei (see Eq. (19)) and the crystalline fraction developed from the instantaneous nuclei and estimate the effect of nucleating agents (see Eqs. (21) and (24)).

To validate the formulae developed, isothermal crystallisation tests on two kinds of PET (vPET and rPET) at two temperatures, PP and LDPE at four temperatures and HDPE at three different temperatures were carried out. Results show that fitting the Advanced Avrami formula provided much better agreement with the measured isothermal crystallisation processes for all the materials tested compared to the classic Avrami equation. The more accurate results by the advanced model could be obtained without making the fitting any more complicated. The additional formulae ministered information not only on the initial I-nucleus fraction and the final I-crystal fraction but also on the time-dependent variation of them making it possible to study and estimate numerically the effect of the nucleating agents. The time-dependent variation calculated made visible that the I-nucleus fraction monotonically decreases with time and the I-crystal fraction tends to an equilibrium formed between the instantaneous and random-nuclei-based crystal fractions about at the half of the total crystallisation time. All of that may assist in the precise planning of the manufacturing technology of the polymer materials. It should be noted that, in practice, the non-isothermal crystallization has been studied in general using DSC measurements and software programs such as the AKTS Thermokinetics Software. Therefore, in our next research, we plan to examine how the new formulas developed by us can be applied to the multi-step isoconversional method according to ICTAC recommendations as kinetic models used for the single-step process.

Authors declaration

The authors of the manuscript **TCA-D-24–00739** entitled:

Advanced Avrami Formula and its Application to Describing the Isothermal Crystallisation of Polymers

Declare the following:

● One author has been designated as the corresponding author and their full contact details (email address, full postal address and phone numbers) have been provided.

● All files have been uploaded, including keywords, figure captions and tables (including a title, description and footnotes) included.

● Spelling and grammar checks have been carried out.

● All references in the article text are cited in the reference list and vice versa.

● Permission has been obtained for the use of any copyrighted material from other sources, including the Web.

● For gold open access articles, all authors understand that they are responsible for payment of the article publishing charge (APC) if the manuscript is accepted. Payment of the APC may be covered by the corresponding author's institution, or the research funder.

CRediT authorship contribution statement

László Mihály Vas: Writing – review & editing, Writing – original draft, Validation, Supervision, Methodology, Formal analysis, Conceptualization. **Emese Slezák:** Writing – original draft, Investigation, Data curation. **Kolos Molnár:** Writing – review & editing, Writing – original draft, Visualization, Methodology, Investigation, Funding acquisition, Data curation. **Ferenc Ronkay:** Writing – review & editing, Writing – original draft, Methodology, Investigation, Data curation.

Declaration of competing interest

The authors declare that they have no known competing financial interests or personal relationships that could have appeared to influence the work reported in this paper.

Acknowledgments

This work was supported by the National Research, Development and Innovation Office, Hungary (2019–1.1.1-PIACI-KFI-2019–00335). This research was supported by the National Research and Development Office (FK 138501), Hungary. Project no. TKP-6–6/PALY-2021 has been implemented with the support provided by the Ministry of Culture and Innovation of Hungary from the National Research, Development and Innovation Fund, financed under the TKP2021-NVA funding scheme.

E. Slezák expresses her gratitude for the project no. KDP-IKT-2023–900-I1–00000957/0000003, which has been implemented with the support provided by the Ministry of Culture and Innovation of Hungary from the National Research, Development and Innovation Fund, financed under the KDP-2023 funding scheme. K. Molnár is grateful for the support of the János Bolyai Scholarship of the Hungarian Academy of Sciences.

Supplementary materials

Supplementary material associated with this article can be found, in the online version, at doi:10.1016/j.tca.2025.179950.

Data availability

Data will be made available on request.

References

[1] C. Schick, R. Androsch, Nucleation-controlled semicrystalline morphology of bulk polymers, Polym. Cryst. 1 (2018), https://doi.org/10.1002/pcr2.10036.
[2] W.N. Dos Santos, J.A. De Sousa, R. Gregorio, Thermal conductivity behaviour of polymers around glass transition and crystalline melting temperatures, Polym. Test. 32 (2013) 987–994, https://doi.org/10.1016/j.polymertesting.2013.05.007.
[3] Y. Lin, E. Bilotti, C.W.M. Bastiaansen, T. Peijs, Transparent semi-crystalline polymeric materials and their nanocomposites: a review, Polym. Eng. Sci. 60 (2020) 2351–2376, https://doi.org/10.1002/pen.25489.
[4] F. Song, Q. Wang, T. Wang, The effects of crystallinity on the mechanical properties and the limiting PV (pressure×velocity) value of PTFE, Tribol. Int. 93 (2016) 1–10, https://doi.org/10.1016/j.triboint.2015.09.017.
[5] C.Y. Li, The rise of semicrystalline polymers and why are they still interesting, Polymer 211 (2020), https://doi.org/10.1016/j.polymer.2020.123150 (Guildf).
[6] H.F.B.C. Brinson, Characteristics, applications and properties of polymers. Polymer Engineering Science and Viscoelasticity: An Introduction, Springer, Boston, 2018, pp. 55–97.
[7] S.S. Sheiko, S.N. Magonov, Scanning probe microscopy of polymers, in: K. Matyjaszewski, M. Möller (Eds.), Polymer Science: A Comprehensive Reference Vol. 1-10, Elsevier, Amsterdam, 2012: pp. 559–605. 10.1016/B978-0-444-53349-4.00047-9.
[8] B. Lotz, What can polymer crystal structure tell about polymer crystallization processes? Eur. Phys. J. E 3 (2000) 181–194, https://doi.org/10.1007/s101890070031.
[9] K. Shirzad, C. Viney, A critical review on applications of the Avrami equation beyond materials science, J. R. Soc. Interface 20 (2023), https://doi.org/10.1098/rsif.2023.0242.
[10] M.A. Arshad, A. Maaroufi, Relationship between Johnson-Mehl-Avrami and Šesták-Berggren models in the kinetics of crystallization in amorphous materials, J. Non Cryst. Solids 413 (2015), https://doi.org/10.1016/j.jnoncrysol.2015.01.012.
[11] A. Gradys, P. Sajkiewicz, A.A. Minakov, S. Adamovsky, C. Schick, T. Hashimoto, K. Saijo, Crystallization of polypropylene at various cooling rates, Mater. Sci. Eng. A (2005) 442–446, https://doi.org/10.1016/j.msea.2005.08.167, 413–414.
[12] U.K. Murmu, J. Adhikari, A. Naskar, D. Dey, A. Roy, A. Ghosh, M. Ghosh, Mechanical properties of crystalline and semicrystalline polymer systems, in: M.S. J. Hashmi (Ed.), Encyclopedia of Materials: Plastics and Polymers, 1st ed., Elsevier, Amsterdam, 2022, pp. 917–927, https://doi.org/10.1016/B978-0-12-820352-1.00248-0.
[13] B. Crist, J.M. Schultz, Polymer spherulites: a critical review, Prog. Polym. Sci. 56 (2016) 1–63, https://doi.org/10.1016/j.progpolymsci.2015.11.006.
[14] A.J. Müller, R.M. Michell, A.T. Lorenzo, Isothermal crystallization kinetics of polymers, Polym. Morphol. Princ. Charact. Process. (2016) 181–203, https://doi.org/10.1002/9781118892756.ch11.
[15] J.N. Hay, Secondary crystallization kinetics, Polym. Cryst. 1 (2018), https://doi.org/10.1002/pcr2.10007.
[16] A. Toda, R. Androsch, C. Schick, Insights into polymer crystallization and melting from fast scanning chip calorimetry, Polymer 91 (2016) 239–263, https://doi.org/10.1016/j.polymer.2016.03.038 (Guildf).
[17] M. Raimo, Growth of spherulites: foundation of the DSC analysis of solidification, ChemTexts 1 (2015) 1–21, https://doi.org/10.1007/s40828-015-0013-1.
[18] C. Berlic, V. Barna, B. Manolescu, D. Dena, Study of the instantaneous nucleation phenomena in soft matter systems by means of Monte Carlo simulation, Dig. J. Nanomater. Biostructures 9 (2014) 197–204.
[19] K. Sugio, S. Tatsuno, H. Fukushima, O. Yanagisawa, Modification of Kolmogorov-Johnson-Mehl-Avrami equation for clustered nucleation, Mater. Trans. 50 (2009), https://doi.org/10.2320/matertrans.M2009025.
[20] J.C. Holzer, K.F. Kelton, Kinetics of the amorphous to icosahedral phase transformation in AlCuV alloys, Acta Metall. Mater. 39 (1991) 1833–1843, https://doi.org/10.1016/0956-7151(91)90152-Q.
[21] J.W. Cahn, The kinetics of grain boundary nucleated reactions, Acta Metall. 4 (1956) 449–459, https://doi.org/10.1016/0001-6160(56)90041-4.
[22] E. Pineda, T. Pradell, D. Crespo, Non-random nucleation and the avrami kinetics, Philos. Mag. A Phys. Condens. Matter, Struct. Defects Mech. Prop. 82 (2002) 107–121, https://doi.org/10.1080/01418610208240000.
[23] Y.L. Chiari, M. Vadlamudi, R. Chella, K. Jeon, R.G. Alamo, Overall crystallization kinetics of polymorphic propylene-ethylene random copolymers: a two-stage parallel model of Avrami kinetics, Polymer 48 (2007) 3170–3182, https://doi.org/10.1016/j.polymer.2007.03.075 (Guildf).
[24] G. Bodor, Structure of polymers, Műszaki Könyvkiadó (1982).
[25] G. Bodor, Structural Investigation of Polymers, joint ed., Akadémiai Kiadó, Budapest, 1991.
[26] B. Wunderlich, Thermal Analysis of Polymeric Materials, 1st ed., Springer, Berlin, Heidelberg, 2005 https://doi.org/10.1007/b137476.
[27] G. Strobl, The Physics of polymers: Concepts for Understanding Their Structures and Behavior, 2007, https://doi.org/10.1007/978-3-540-68411-4.
[28] G. Reiter, G.R. Strobl (Eds.), Progress in Understanding of Polymer Crystallization, Springer, New York, New York, 2007, https://doi.org/10.1007/3-540-47307-6.
[29] M. Fanfoni, M. Tomellini, The Johnson-Mehl-Avrami-Kolmogorov model: a brief review, Nuovo Cim. Della Soc. Ital. Di Fis. D Condens. Matter At. Mol. Chem. Phys. Biophys. 20 (1998) 1171–1182, https://doi.org/10.1007/BF03185527.
[30] A.T. Lorenzo, M.L. Arnal, J. Albuerne, A.J. Müller, DSC isothermal polymer crystallization kinetics measurements and the use of the Avrami equation to fit the data: guidelines to avoid common problems, Polym. Test. 26 (2007) 222–231, https://doi.org/10.1016/j.polymertesting.2006.10.005.

[31] J. Lieblein, G.A. Korn, T.M. Korn, Mathematical Handbook for Scientists and Engineers, McGraw-Hill, East Lansing, 1961, https://doi.org/10.2307/2003035.
[32] K. Bocz, F. Ronkay, K.E. Decsov, B. Molnár, G. Marosi, Application of low-grade recyclate to enhance reactive toughening of poly(ethylene terephthalate), Polym. Degrad. Stab. 185 (2021), https://doi.org/10.1016/j.polymdegradstab.2021.109505.
[33] F.J. Lanyi, N. Wenzke, J. Kaschta, D.W. Schubert, On the determination of the enthalpy of fusion of α-crystalline isotactic polypropylene using differential scanning calorimetry, X-ray diffraction, and fourier-transform infrared spectroscopy: an old story revisited, Adv. Eng. Mater. 22 (2020), https://doi.org/10.1002/adem.201900796.
[34] A.A. Gaonkar, V.V. Murudkar, V.D. Deshpande, Comparison of crystallization kinetics of polyethylene terephthalate (PET) and reorganized PET, Thermochim. Acta 683 (2020), https://doi.org/10.1016/j.tca.2019.178472.
[35] F.N. Andrade, R. Fulchiron, F. Collas, T.F.L. McKenna, Condensed mode cooling for ethylene polymerization: part V—Reduction of the crystallization rate of HDPE in the presence of induced condensing agents, Macromol. Chem. Phys. 220 (2019), https://doi.org/10.1002/macp.201800563.
[36] L.A. Baldenegro-Perez, D. Navarro-Rodriguez, F.J. Medellin-Rodriguez, B. Hsiao, C. A. Avila-Orta, I. Sics, Molecular weight and crystallization temperature effects on poly(ethylene terephthalate) (PET) homopolymers, an isothermal crystallization analysis, Polymers 6 (2014) 583–600, https://doi.org/10.3390/polym6020583 (Basel).